agriculture

MDPI

Article

New, Low-Cost, Hand-Held Multispectral Device for In-Field Fruit-Ripening Assessment

Miguel Noguera [1,*], Borja Millan [2] and José Manuel Andújar [1]

[1] Centro de Investigación en Tecnología, Energía y Sostenibilidad (CITES), Universidad de Huelva, La Rábida, Palos de la Frontera, 21819 Huelva, Spain
[2] Departamento de Ingeniería Eléctrica, Electrónica, Informática y de Sistemas, Universidad de Oviedo, C/ Pedro Puig Adam, 33203 Gijón, Spain
* Correspondence: miguel.noguera@diesia.uhu.es

Abstract: The state of ripeness at harvest is a key piece of information for growers as it determines the market price of the yield. This has been traditionally assessed by destructive chemical methods, which lead to low-spatiotemporal resolution in the monitorization of crop development and poor responsiveness for growers. These limitations have shifted the focus to remote-sensing, spectroscopy-based approaches. However, most of the research focusing on these approaches has been accomplished with expensive equipment, which is exorbitant for most users. To combat this issue, this work presents a low-cost, hand-held, multispectral device with original hardware specially designed to face the complexity related to in-field use. The proposed device is based on a development board (AS7265x, AMS AG) that has three sensor chips with a spectral response of eighteen channels in a range from 410 to 940 nm. The proposed device was evaluated in a red-grape field experiment. Briefly, it was used to acquire the spectral signature of eighty red-grape samples in the vineyard. Subsequently, the grape samples were analysed using standard chemical methods to generate ground-truth values of ripening status indicators (soluble solid content (SSC) and titratable acidity (TA)). The eighteen pre-process reflectance measurements were used as input for training artificial neural network models to estimate the two target parameters (SSC and TA). The developed estimation models were evaluated through a leave-one-out cross-validation approach obtaining promising results (R^2 = 0.70, RMSE = 1.21 for SSC; and R^2 = 0.67, RMSE = 0.91 for TA).

Keywords: sensor; multispectral; precision farming; machine learning; artificial neural network; AS7265x

Citation: Noguera, M.; Millan, B.; Andújar, J.M. New, Low-Cost, Hand-Held Multispectral Device for In-Field Fruit-Ripening Assessment. *Agriculture* **2023**, *13*, 4. https://doi.org/10.3390/agriculture13010004

Academic Editors: Ahmed Mustafa Rady and Ewa Ropelewska

Received: 15 November 2022
Revised: 16 December 2022
Accepted: 18 December 2022
Published: 20 December 2022

1. Introduction

Fruit ripening involves a set of morphological, physiological, and biochemical changes that make fruit suitable for consumption. During maturation, a green, firm, immature fruit usually becomes more colourful, softer, sweeter, and aromatic. Furthermore, biotic and abiotic stresses trigger metabolic processes that reduce fruit quality not only during growth but also during harvest and storage [1]. These modifications can be characterized through physical and chemical attributes such as size, shape, texture, firmness, soluble-solids content (SSC), starch, sugars, acids, oils, internal ethylene concentration, external and internal colour, and concentration of chlorophyll, etc. [2]. Thus, there are objective parameters which allow for the monitoring of the quality state of fruit and the carrying out of actions to improve it. Traditionally, the assessment of these fruit-quality indicators has been based on chemical and physical methods, such as high-performance liquid chromatography (HPLC), refractometry, and colorimetry, among others. These kinds of methods require extensive sample preparation, expert workers, and advanced laboratory facilities. All these factors lead to a high cost. Therefore, there are two main concerns accompanying these methods. These include the representativeness of a sample

from a field on a given date and the number of sample dates that can be performed during the campaign. These concerns lead to poor temporal and spatial resolution in the monitorization, which limits the growers' reaction capacities. These facts make the implementation of rapid, economical, and non-destructive alternatives necessary, as they would benefit growers, processors, and consumers alike. The in-field, non-destructive assessment of fruit ripeness would provide numerous benefits compared to traditional destructive techniques such as high-throughput assessment, simultaneous multiple measurements, and real-time decision making.

In recent decades, spectral-based approaches have been proposed as an alternative to fruit-quality assessment because of their speed and non-invasive character [3]. The theorical foundation of this kind of method relies on the interaction between light and objects. Briefly, every molecule consists of several atoms. The bonds between the atoms can be excited by light with a characteristic wavelength (i.e., colour) [4,5]. This leads to short time vibrations within the molecule. This specific wavelength depends on the strength of the bonds and the mass of the atoms and is unique for each molecule. This interaction between light and objects can be assessed by analysing the three processes of absorption, reflection, and transmission. As no two organic compounds have the same characteristics, a compound can be identified accurately by analysing its absorption spectrum and matching it with a database [4].

The complexity of the interaction between light and objects has led to several lines of research, such as fluorescence spectroscopy [6], Raman spectroscopy [7], multispectral imaging [8], hyperspectral imaging [9], and visible, near-infrared (VIS-NIR) 'point' spectroscopy [10]. All the referenced works have demonstrated the suitability of light-based approaches for agricultural applications and specifically fruit-quality assessment. The present work is centred on VIS-NIR 'point' spectroscopy. The particularity of point spectroscopy in terms of spectral imaging is the resolution. While spectral cameras offer images composed of numerous pixels containing information, which allow for contrast in different parts of the sample, the 'point' sensors give just one measure for the focused area.

The use of VIS-NIR spectroscopy for the characterization of agri-food products is a relatively mature topic, even more so regarding precision farming. The combination of chemometrics techniques with spectral data has been widely studied. Fifteen years have passed since the comprehensive review on the use of NIR spectroscopy for non-destructive quality assessment of fruits and vegetables by Nicolaï et al. (2007). The state of the art has been expanded following this review, with works focused on the monitorization of different biophysical parameters beyond the quality status of fruits [3,11–14]. In fact, there are various commercially available instruments dedicated to the post-harvest sector. In this sense, VIS-NIR spectrophotometers have been integrated into commercial packing lines. Additionally, there is also commercially available hand-held equipment for fruit analyses. However, this equipment is very expensive—even exorbitant—for most users. In recent decades, the improvement in the microelectronic industry has resulted in lower costs and improved component features. This development is arousing an increasing interest in the use of low-cost spectral sensors for agricultural applications [15–17], as this would allow for the implementation of these non-destructive methodologies throughout the post-harvest value chain, both upstream (to the field) and downstream (to distribution centres and to consumer use). Thus, there is room to confirm past work and to further improve these processes to underpin adoption.

In this context, this work presents a custom-built, low-cost multispectral device designed especially for in-field applications. The proposed device is based on the "AS7265x" development board (AMS AG). This sensor has been previously tested for agricultural applications. Moinard et al. [18] proved its potential for estimating the percentage of grass cover and estimating vine vigour. Noguera et al. [17] used it to assess the quality status of intact olive fruits under laboratory conditions with promising results. Zhang et al. [19] evaluated it for classifying apples in three ripening categories based on classical maturity indicators. Leon-salas et al. [20] used it to determine photosynthetically active radiation

indoors and outdoors. Furthermore, there are other works centred in sensors with similar features. For example, Trang et al. [21] developed and tested a device based on six-channel NIR sensors (AS7263, AMS AG) for measuring chlorophyll content in a leaf. Li et al. [22] evaluated a commercially available spectral sensor (SCIO) to predict the quality of kiwifruit, apples, feijoas, and avocados. These sensors have the potential to provide objective information to growers. However, most of the previously mentioned works that focused on the use of spectroscopy for fruit quality assessment were conducted under laboratory conditions. This approach allows for the control of external parameters and reduces both the complexity of the problem and the applicability of the solution. Further, the limited works focused on in-field solutions used equipment with very high acquisition costs. Therefore, the goal of this research is to develop a hand-held spectral device, affordable for all kinds of users (growers, processors, and consumers), and to continue exploring its potential for in-field applications. Thus, a prototype was developed with hardware (described in Section 2.2) that was specially designed to acquire data under field conditions. In order to evaluate its suitability, an experiment was designed with the goal of estimating the quality parameters of grapes by means of spectral data acquired with the proposed device under field conditions.

2. Materials and Methods

2.1. Device Description

The multispectral sensor device is composed of different elements that are assembled inside a 3D-printed enclosure. The objective was to develop a tool that is reliable and easy to operate under field conditions by non-specialized personnel. To reduce cost and simplify maintenance, commercial components were selected where available. However, some PCBs (printed circuit boards) were developed to simplify the assembly. A description of the different components is presented in the following sections, introducing the hardware and the software that controls the operation of the sensor.

2.1.1. Hardware: Electronic components

- AMS AS7265x development board (AMS AG, Premstätten, Austria): This board is composed of three main chips: AS72651, AS72652, and AS72653. These chips are sensible to six different bands (by including six optical filters each) in the range between 410 nm and 940 nm, with a full width at half maximum (FWHM) of 20 nm. The AS72651 acts as a master for the chip arrangement and the communication with the rest of the components is performed with this chip. This development board results in a low-cost, 18-channel multispectral sensor.
- Arduino MKRZero Board (Arduino LLC, Monza, Italy): The Arduino MKR Zero board was selected because of its small form factor, low power consumption, low cost, and the availability of an SD card slot. A custom software was developed using the Arduino IDE (described in the software section). This board communicates with the AS7265x development board, OLED screen, and LED PCB to perform data acquisition.
- Interconnection board: There is a high number of interconnected components on the system. An interconnection board was designed and manufactured to generate a reliable connection between them. This board serves as the core of the system, adapting the voltage from the battery, regulating LEDs' signal intensity, and interfacing the different components of the sensor with connectors to different subsystems. A constant-current LED driver (RCD-24, RECOM, Germany) installed on the PCB allows us to modulate capturing parameters (light intensity and power on time) ,controlled by the Arduino MKR. A schema of the different connections between device components is depicted below (Figure 1).

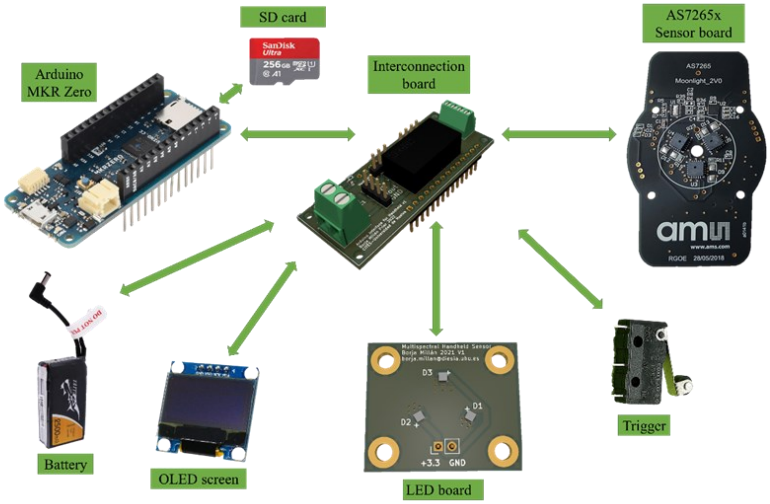

Figure 1. Schema of the different components of the low-cost multispectral device, including the interconnections between them.

- LED PCB: The samples to be measured must be illuminated to obtain the reflectance measurement. An array of three IR-broadband LED emitters (OSLON P1616 SFH 4737, OSRAM, Germany), was used to achieve this goal. This component was developed specifically for spectroscopy applications, providing a wide emission spectrum in the VNIR with the advantage of less power and heat dissipation requirements than a halogen lamp. The PCB allows us to install three LEDs and easily attaches to the 3D-printed reflective dome of the instrument. Although the LEDs are only powered when a measurement is taken, the PCB also acts as a heat dissipator to reduce the damage to this component due to heat build-up.
- OLED Screen: The screen serves as a guide for the user during measurement. The developed device included an OLED display, specifically a 1.3-inch panel with a resolution of 128 by 64 pixels. The availability of an integrated display avoids the necessity of a computer or some other external device to verify the status of the device and its proper operation in the field. The screen shows real-time data, the file name, the number of measurements taken, and the configuration parameters (Figure 2).

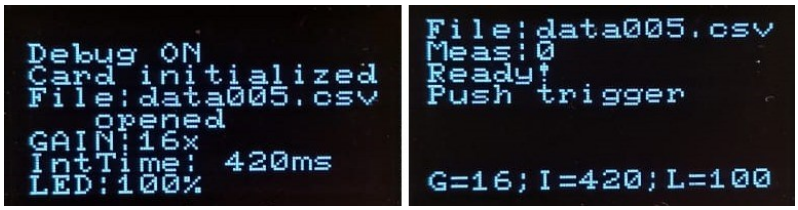

Figure 2. Image of the device's integrated OLED screen showing initialization data (**left**) and ready to perform data capture (**right**).

- Battery: The system can be powered from any DC source up to 35 V through a barrel connector (2.1 × 5.5 mm). During the experiments, the prototype was powered by a 2s LiPo (Lithium-ion Polymer) battery connected to the device controller board. The low-power consumption of the sensor allows for extended operation time lasting beyond a workday. In any case, the battery is placed outside the device, so it is easy to replace the depleted battery and continue capturing data in the field.

2.1.2. Hardware: 3D-Printed Enclosure

In order to provide a compact, ergonomic, and low-cost enclosure, a device case was designed using FreeCAD 0.19 (Figure 3) and manufactured with a 3D printer using a biodegradable polylactic acid (PLA) filament. Four different components were designed:

- Main enclosure: A box-type enclosure was designed as the main body of the device. The AMS AS7265x development board, Arduino MKR Zero, and interconnection board are stacked inside and held in place with help from two 3D-printed separators.
- Lid with screen: This lid seals the sensor to allow in-field operation. The OLED screen is fixed to the lid of the main enclosure, and its position allows for easy visualization of the data when taking a measurement.
- Reflective dome and diffuser bracket: A dome that holds the light source (LED PCB) and integrates a light-diffusion film (OptSaver L-9960, Kimoto LDT, Switzerland). The diffuser is placed in front of the sensor to homogenize the illumination and the signal measured an obtain a representative measurement. Data acquisition is performed by making contact between the sample and the diffusive film. The dome is developed to guarantee that the sample is placed at a 45° angle with the light source and the sensor.
- Handle with trigger: This part allows for the simultaneous support and operation of the device with one hand (enabling the use of the other hand for sample manipulation). An end stop switch is used as a trigger. The switch is installed inside the handle and the wires to connect to the interconnection board are conducted inside the handle to the main enclosure.

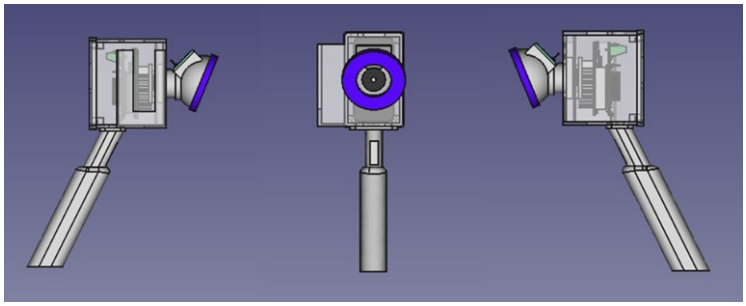

Figure 3. Three-dimensional rendering of different views of the device case designed with FreeCAD 0.19.

2.1.3. Software

The Arduino MKR board was programmed using Arduino IDE. A diagram of software functionality is depicted in Figure 4. At boot, the system will check for a file "UPDATE.bin" in the SD. In the case this file is available, the firmware is updated and the board is rebooted. This allows for a reconfiguration of different parameters of the system without the need for a connection with a PC.

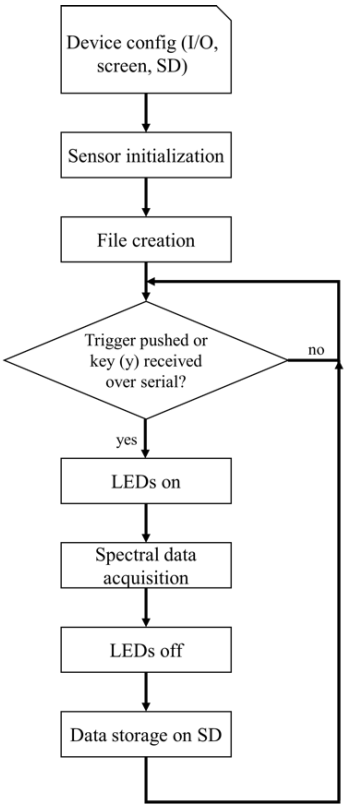

Figure 4. Flow chart of the process for multispectral data capture.

The software operation can be summarized in the following steps:

- The first step is the initialization of all the components of the system, including the input/output configuration and the serial comm parameters definition. Two main serial connections are defined: a connection with the AMS AS7265x development board and with a computer to allow for device control and data monitorization over a computer. Moreover, the OLED screen is connected by a SPI (Serial Peripheral Interface).
- The sensor board (AMS AS7265x) is configured using AT commands over a serial port. Primarily, sensor gain and integration time must be established. Other parameters for calibration can also be configured. All the initialization steps are displayed on the OLED Screen and optionally on the serial connection using a virtual comm over USB. This allows the user to quickly debug any failures during the configuration (i.e., a lost connection with the sensor).
- The next step is to initiate the SD card. A scan of the contents of the card is performed, and a new file is created with the format "dataXXX.csv" where XXX is the last file number stored plus one. Every time the device is powered-up a new file is created, preserving the previously acquired data. The file has a header with a description of the configuration used (mainly integration time, gain, and LED current). The captured spectrum is stored as one measurement per row with reflectance separated by a comma, allowing the file to be processed by standard software compatible with CSV file format.
- After the initialization is completed, the system waits for user input in which the trigger is pressed or a command is sent via serial connection. This dual implementation allows for the control of the system autonomously in the field (via the trigger) or through a connection to a computer, which can be more interesting for in-laboratory operation as it allows for real-time supervision of the measurements.
- When an input is detected, the device begins the capturing process:
    - LEDs are turned on with the configured current at 0–1000 mA.

- A command is sent to the AMS AS7265X sensor board to perform the acquisition, and the system waits for correct data reception.
- The LEDs are turned off as soon as all the data are received.
- Finally, the data are stored in the SD card. Following this, the system is ready for another measurement.

All the data are stored as soon as they are received, reducing the time spent waiting until data has been written to the SD card. This process minimizes information loss in case the power is removed after an acquisition is performed. Additionally, the device can be turned off by removing the power without any special procedure. The only precaution needed to turn off the device (and avoid data corruption) is to allow the system to store the last measurement.

2.2. Validation Experiment

In order to evaluate the suitability of the developed device, an experiment was carried out that was intended to assess ripening indicators of grape berries (*Vitis vinifera* L.) by means of the spectral data acquired with the device under field conditions.

2.2.1. Study Site Description

The study site was situated in the *Condado de Huelva* appellation (Bodegas Contreras Ruiz, S.L, Rociana del Condado, Huelva). It is a commercial vineyard of *Syrah* variety, which is a red-grape variety widely used in the wine industry. The experimental field had an extension of approximately 1000 m^2. The soil in the study area is characterized by a heterogeneous structure and composition. Thus, it presents sandy loam areas alternating with clay-loam zones. This irregular pattern relating to the structure and composition of the soil is reflected in the physiology of the plants. There were plants with different paces of ripening, which resulted in high variability according to the quality parameters considered in this research. This was a key factor for the validation experiment, as variability regarding the target parameters is essential to assure the generalization capacity of the developed estimation models.

2.2.2. Spectral Collection

The field experiment was performed on 22 July 2021. This date was selected for its proximity to the optimum harvest time according to the winery's manager. The first part of the experiment was performed in the vineyard and consisted of a sample collection. To obtain the most variability in terms of the ripening stage of the grapes, the entire vineyard was covered by randomly collecting a total of 80 samples. A grape cluster was considered as a sample unit. Each of the grape clusters was harvested using pruning shears. The spectral signature of the cluster was acquired immediately after harvest. The measuring methodology involved facing the dome of the device against the upper part of the grape cluster and making a capture. The measurements were made in the centre of the row to avoid plant shadows on the sample (Figure 5). Two captures were acquired per sample, taking the average reflectance of the two spectra as representative data for each sample. After being processed, each sample was packaged, labelled, and refrigerated at 3–4 °C in a portable cooler during its transport to laboratory. At the laboratory, the samples were analysed on the same day as the sample collection. Once every fifteen samples, three captures of a surface of known reflectance (Labsphere, Inc, North Sutton, NH, USA) (53% calibrated reflectance) were taken. The average signal of the three captures would be used later as a reference to normalise the following fifteen samples. This enabled the prevention of subsequent errors due to variations in ambient light.

Figure 5. Methodology for spectral data acquisition.

2.2.3. Reference Analysis

The development of estimation models by means of sensor-acquired spectral data requires a reference dataset that indicates the actual state of the samples regarding the target parameters. With this purpose, the samples were subjected to destructive chemical methods to obtain objective indicators of their actual ripening status. In this work, solid soluble content (SSC) and titratable acidity (TA) were used as target parameters, given that they are routinely considered by the wine industry to determine the ripening status of grapes [23]. The SSC is defined as the total content of solids dissolved in a given volume of juice. This includes carbohydrates, organic acids, proteins, fats, and minerals. However, in a grape at a certain grade of maturity, sugars represent around 90–95% of the total solid, so SSC is also considered a good approximation of sugar content (sweetness). Furthermore, the SSC of the grapes in the harvest is directly related to the alcoholic grade of the wine to be produced [24]. TA is defined as the degree of acidity of a substance and is measured by volumetric methods. In the case of grapes, this parameter is correlated to the SSC; as the fruit ripens, the SSC content increases while the TA decreases. The balance between these two grape parameters at the moment of harvest is decisive of the features of the wine to be produced, which means that controlling these parameters is paramount [23].

The methodologies employed to assess both ripening indicators are standardised by the International Organization of Vine and Wine (OIV) [25]. The first step of the procedure to determine SSC and TA values was the shelling of the grape clusters. Following shelling, fifty grapes per cluster were randomly selected and were then squeezed to obtain the wort. Just a few drops of wort were used to determine the SSC (Brix°) by means of a temperature-compensating digital refractometer (HI96801, Hanna instruments, Spain). On the other hand, an initial volume of 50 mL of wort per sample was used to assess grape TA by titration with 0.1 NaOH to an end point of pH 7.0 using an automatic titralyser (LDS1155500, Dujardin-Salleron, France). The results were expressed as g/L of Chlorohydric acid. The statistics (the range, mean, and standard deviation (SD)) of both parameters were analysed using the Orange 3 software [26].

2.3. Methodology for Ripening Status Estimation from Multispectral Information

2.3.1. Data Pre-Processing

The mean reflectance signature of each grape sample was calibrated to avoid eventual errors due to variations in the ambient light. The calibration consisted of a normalisation, using as reference the spectral signature of the known reflectance surface (53%) (Labsphere, Inc, North Sutton, NH, USA), which was captured once every fifteen samples.

The level of reflectance of the known reflectance surface (53%) allowed the attainment of a better resolution as the reflectance of the samples was less than 50% for all the considered bands. The eighteen reflectance signals of the known reflectance surface were used as reference for calibrating the spectral response of the subsequent fifteen samples according to the next equation:

$$\mathrm{Rcal}_{\mathrm{wl}} = \frac{\mathrm{R}_{\mathrm{wl}}}{\mathrm{Rref}_{\mathrm{wl}}/0.53} \quad (1)$$

where R_{wl} is the reflectance value measured for a given spectral band in a capture of a sample, $Rref_{wl}$ is the reflectance value measured for that spectral band in the previous capture of the known reflectance surface, and $Rcal_{wl}$ is the corrected value of reflectance in the sample for the given band.

2.3.2. Estimation Model Development

The corrected reflectance of the eighteen spectral bands captured by the sensor were used as input variables to train two artificial neural networks (ANN) to estimate the SSC and TA. An ANN is a non-linear, non-parametric method (machine learning method). This approach consists of a structure of neurons linked together and arranged in layers. The neurons of different layers are interconnected, and each connection has a specific weight. Each neuron essentially realises a linear regression followed by a non-linear function. Briefly, the ANN architecture works to minimize the mean–square deviation trough the error-correction learning rule. Thus, the error will be minimized by adjusting the weight of each layer of neurons. These characteristics allow for an extraordinary connection between complex spectral information and key parameters without any constraint on the sample distribution. This makes ANN approaches appropriate to define complex non-linear relationships that normally exist between spectral signatures of fruits and ripening indicators.

In this work, the software used for data processing and ANN training was Orange 3 [26]. This is an open-source tool for data visualization, pre-processing, and modelling. The ANN used was a multi-layer perceptron (MLP) algorithm with back propagation. The architecture of the neural network employed was composed of a hidden layer with six neurons, eighteen inputs, and one output (one model per target parameter). Identity was used as an activation function for the hidden layer, and an L-BFGS-B (an optimizer in the family of quasi-Newton methods) was used as a Solver for weight optimization. Before the feeding of the ANN model, the dataset was processed with a local outlier factor algorithm. This algorithm computes a score reflecting the degree of abnormality of the observations. It measures the local density deviation of a given data point with respect to its neighbours. The contamination (proportion of outlier in the dataset) was set at 2%, so this previous analysis discarded two samples. Figure 6 shows the workflow of the models. Leave-one-out cross-validation (LOOCV) was used as a validation method, due to it being considered the most suitable due to the volume of the dataset (n = 80). This method holds out one instance at a time, inducing the model from all others and then estimating the held-out instances. This method is obviously very stable and suitable for limited volume datasets as it avoids over-fitting. Alternatively, a random sampling (RS) test was made. For that purpose, the complete data set was randomly divided into two subsets: 75% training and 25% external validation (test). The training was repeated two consecutive times, obtaining a test set of 40 samples.

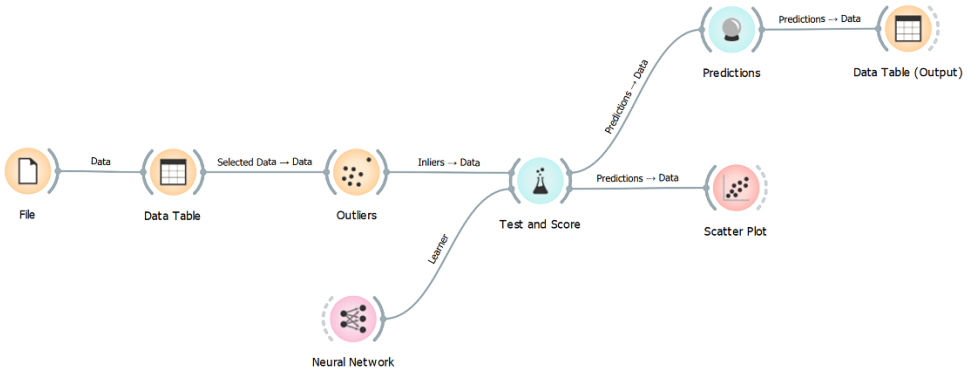

Figure 6. Simulated workflow of the model in Orange 3 data-mining software.

2.4. Criteria for Model Performance Evaluation

The performance of the estimation models was measured by the coefficient of determination (R^2), and the root–mean–square error of prediction (RMSE) between the actual values of the ripening indicators determined by chemical methods and those estimated by ANN models. In the case of LOOCV, the output of the ANN applied to the validation set excluded during training at every iteration was used to determine the mentioned statistical parameters. Thus, a test set of 80 predictions was configured. The coefficient of determination (R^2) was used to assess the relationship between the actual and predicted target parameters. On the other hand, the RMSE is the standard deviation of the residuals (prediction errors). Residuals are a measure of the distance of data points to the regression line; RMSE is a measure of how spread out these residuals are. In summary, higher R^2 and smaller RMSE values indicated better model performance.

RMSE can be mathematically formulated as:

$$\mathrm{RMSE} = \sqrt{\sum_{i=1}^{n} \frac{(\mathrm{Ypred_i} - \mathrm{Yref_i})^2}{n}} \quad (2)$$

where Y_{predi} is the response of the model, Y_{refi} is the reference data, and n is the number of measurements in the respective external-validation dataset. Furthermore, it also was considered the coefficient of variation of the RMSE (CVRMSE), which is the result of normalizing the RMSE by the mean value of the measurement. This allows for the avoidance of ambiguity, facilitating the comparison between datasets or models with different scales.

Additionally, paired samples (*t*-tests) for dependent samples were also conducted to confirm the results from the R^2, RMSE, and CVRMSE analyses. For this purpose, the data pairs of the output of the ANN and the validation data excluded during training at every iteration of the LOOCV, the reference value, and the resulting prediction corresponding to the external validation sets in the case of the RS were compared. The paired t-test is a parametric method, useful for testing whether the means of two groups are different when the samples are drawn in pairs. The *t*-test was carried out using Microsoft® Excel® for Microsoft 365 MSO (version 2211) software. The compliance with the null Hypothesis in this test ($p > 0.05$) indicates that there were no significative differences between the mean of the measures based on the proposed device and the obtained through the reference methods.

3. Results

3.1. Actual Quality Status of Grape Samples

A total of 80 grape samples of the Syrah variety were considered in this research. Table 1 summarizes the statistical details of the whole dataset related to the explored ripening indicators. In the case of soluble solid content (SSC) (expressed as °Brix), the grape

samples varied between 10.4° and 19°, with an average value of 16 ± 1.9°. On the other hand, the titratable acidity (TA) (expressed as g/L of Chlorohydric acid), of the grape samples ranged between 2.7 g/L and 10.9 g/L with an average value of 5.1 ± 1.5 g/L. The ranges of both parameters were quite wide, with grape clusters close to the optimum state for harvest and grape clusters with a further-delayed ripening state. On the other hand, a regression between both ripening indicators showed a coefficient of determination (R^2) of 0.67 between both, indicating a correlation between both parameters.

Table 1. Statistics (range, mean, and standard deviation (SD)) of the grape dataset related to SSC and TA.

	Range	Mean	SD
SSC (°Brix)	10.4–19	16.1	1.87
TA (g/L Chlorohydric acid)	2.7–10.9	5.1	1.50

3.2. Spectral Signature of Samples

In order to detect clear differences in the spectral response of the grapes related to the target parameters, a visual inspection of the spectral responses of the samples situated in the limits of the histograms was undertaken. Figure 7 represents the reflectance response corresponding to approximately the 10th and above the 90th percentile of the histogram of the SSC (a) and TA (b). Similarity between the spectral responses related to both ripening indicators was most remarkable. However, this fact may be due to the correlation between both parameters during the ripening process ($R^2 = 0.67$). If we attend to the differences in the spectral response related to the levels of both parameters, an increment of reflectance can be observed in the samples with high levels of SSC and low levels of TA. These reflectance peaks were especially noticeable between 410–680 nm and 860–940 nm, which includes the visible domain, and the further away bands of the red edge.

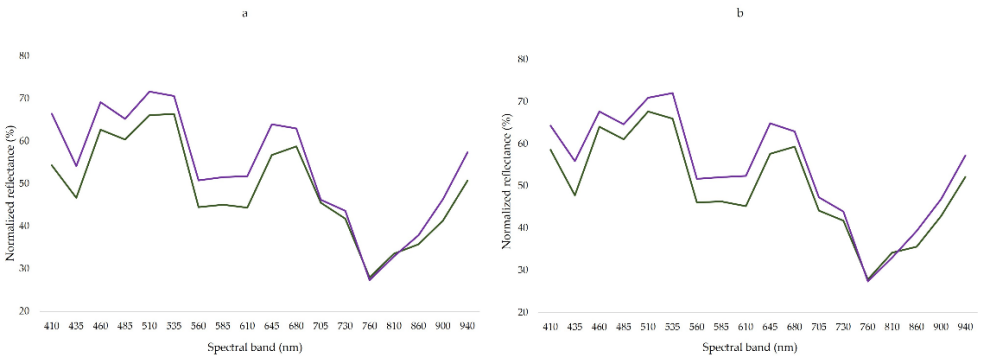

Figure 7. Mean reflectance responses of grape clusters with an advanced ripening state (purple) and an initial state (green) relating their levels of SSC (**a**) and TA (**b**). Each line includes the mean reflectance of eight samples (corresponding to approximately the 10th and above the 90th percentile, respectively, for each parameter).

3.3. Evaluation of the Performance of the Estimation Models

The performance of the ANN models was evaluated based on an LOOCV and a random-sampling (RS) test. Table 2 shows the statistics between the output of the ANN and the validation data excluded during training at every iteration in the case of LOOCV and the external validation set in the case of RS. The goodness-of-fit of the estimation models was similar for the two target parameters. This fact may be due to an inter-correlation between the two target parameters ($R^2 = 0.67$). In the LOOCV, the output of the ANN model showed a good relationship between the values of the target parameters determined by standard methods (SSC and TA), with coefficients of determination of 0.70 for SSC and 0.67 for TA (Figure 8). In this instance, the RMSE was 1.00 (Brix°) for the estimation of SSC, and 0.83 (g/L Chlorohydric acid) for TA. When normalising the RMSE value

by the mean of the measurement (CVRMSE), it was found that the RMSE supposed a 6% respect to the mean for the estimation of the SSC and a 16% for the estimation of the TA. The above-mentioned metrics were supported by the *p*-value obtained in the paired samples *t*-test ($p = 0.15$ for SSC and $p = 0.66$ for TA).

On the other hand, the RS displayed better performance in terms of coefficients of determination ($R^2 = 0.72$ for SSC and $R^2 = 0.74$ for TA). However, the RMSE slightly increased (RMSE = 1.1 for SSC and RMSE = 0.84), being 7% with respect to the mean in the case of SSC and 17% in the case of TA. Again, the *p*-values obtained in the paired samples t-test ($p = 0.20$ for SSC, and $p = 0.53$ for TA) were over the significance limit ($p = 0.05$) in both cases.

Table 2. R^2, RMSE, CVRMSE, and *p* (*p*-value from paired samples *t*-test) between reference values of SSC and TA, measured by chemical methods, and those estimated based on ANN approaches during the LOOCV and random sampling.

	LOOCV				Random Sampling			
	R^2	RMSE	CVRMSE	*p*	R^2	RMSE	CVRMSE	*p*
SSC (°Brix)	0.70	1.00	0.06	0.15	0.72	1.1	0.07	0.20
TA (g/L Chlorohydric acid)	0.67	0.83	0.16	0.66	0.74	0.84	0.17	0.53

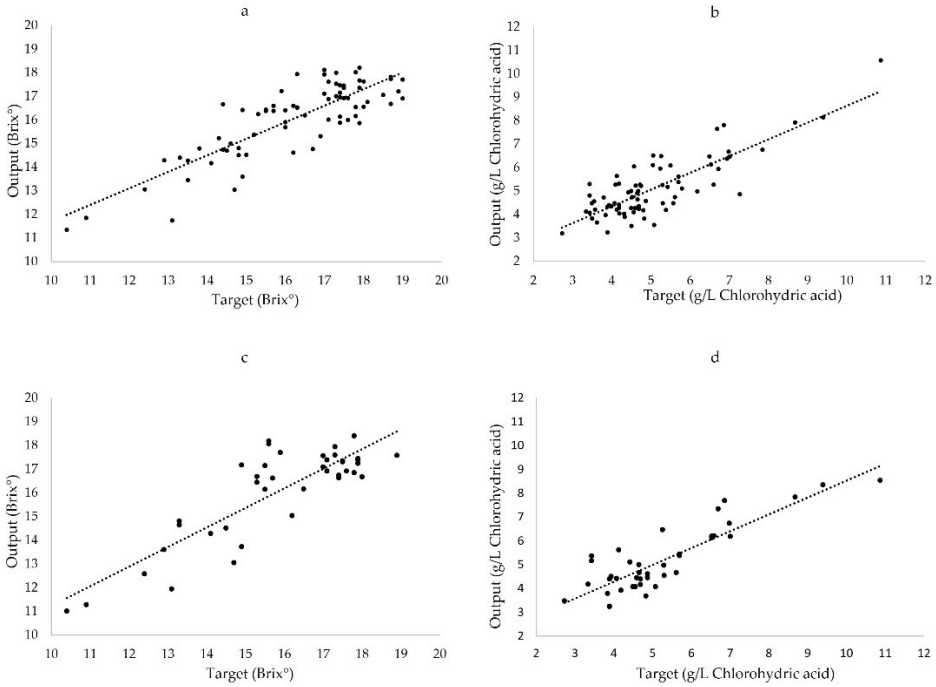

Figure 8. Output of the ANN models versus the validation data excluded during training at every iteration of the LOOCV (SSC (**a**) and TA (**b**)) and random sampling (SSC (**c**) and TA (**d**)).

4. Discussion

This work presents a custom-built, low-cost multispectral device specially designed for fruit-quality assessment under field conditions. In order to evaluate the suitability of the proposed device, an experiment aimed to estimate quality indicators of red grapes was performed. The selected target-quality indicators were the solid soluble content (SSC) and the titratable acidity (TA). The experiment consisted of a sample collection in a red-grape vineyard. The proposed multispectral sensor was used to collect the spectral signature of the samples under field conditions. Subsequently, the samples were packed in zip bags, tagged, and carried to the laboratory, where they were processed through destructive chemical methods to obtain ground-truth values of the target quality indicators. Finally, these quality indicators were used as a target to train artificial neural network

(ANN) models using the corrected reflectance of the eighteen spectral bands captured by the sensor as inputs.

Prior to the model generation, a visual inspection of the spectral fingerprint of the samples was carried out to detect evidence of the correlation between the target parameters and the spectral signatures of the samples (Section 3.2). This previous analysis was based on the samples at the 10th and the 90th percentiles of the SSC and TA histograms. At first sight, the similarity of the spectral signature related to both ripening indicators stood out. This fact may be due to the correlation between both parameters (R^2 = 0.67). This correlation is due to the fact that grape maturation leads to an increase in SSC levels as the TA level decreases [23]. On the other hand, the analysis related to the influence of the levels of both parameters on the spectral signature of the samples showed overtones between 410–680 nm and 860–940 nm in the samples with high levels of SSC and low TA with respect to the samples with low SSC and high TA. The spectral range between 410–680 nm encompasses the visible domain (VIS), so the overtones in these wavelengths may be due to a correlation between the colouration changes of the grapes during ripening (the accumulation of red pigments—carotenoids and anthocyanins,—and chlorophyll a and b) and the levels of both parameters [2]. Furthermore, the spectral range between 860–940 nm covers a part of the NIR domain, which is associated with the first and second overtones of O–H stretching [10]. Therefore, the overtones observed in that spectral region may be due to variations in the water content of the samples, which is related to the values of the target parameter. In addition, it is expected that sugars absorb at the spectral range between 740–984 nm [24]. These facts may explain the effect of the SSC and TA on the spectral signal of the samples identified in the previous visual inspection (Section 3.2). Machine learning methods—and concretely, ANN—have the capability to capture non-linear relationships between related parameters without explicitly knowing the underlying data distribution. The use of an ANNs makes having a precise knowledge about how spectral information and the target parameters are related unnecessary. So, although the reflectance signal of the samples in the spectral bands between 705 - 810 nm seemed to be less affected by the target parameters, they were finally considered in the estimation models as their exclusion did not improve the model's performance. Therefore, the corrected reflectance in the eighteen bands acquired by the sensors were used to train two ANN models aimed at estimating the SSC and the TA of the grapes. A leave-one-out cross-validation (LOOCV) algorithm was used as a validation method. This method uses a single observation from the original sample as the validation data and uses the remaining observations as training data. This is repeated for the entire dataset. After applying an LOOCV, the whole dataset participates in both training and validation. Thus, LOOCV avoids the uncertainty arising from the random division of the dataset into training and external validation (test) subgroups. As there is no random disaggregation of the data, the LOOCV results are fully reproducible. For this reason, LOOCV was considered the most suitable validation method for this research, especially considering that the limited volume of the dataset (n = 80) allowed for the use of a processing-intensive methodology such as LOOCV. As an alternative to the LOOCV, a random-sampling test was applied in order to confirm the performance observed in the LOOCV.

The obtained results were promising. In the case of the SSC, the LOOCV showed a good performance of the ANN model with a coefficient of determination (R^2) between the estimated and the actual values of the SSC of 0.70, and a root–mean–square error (RMSE) of 1.00, which supposed the 6% of the mean value of the measurement (CVRMSE = 0.06). These metrics indicated a good predictive potential and were supported by the *p*-value obtained in the paired samples t-test (p = 0.15), which was higher than the significance limit (p = 0.05). This argues for the similarity between the means of the measures obtained by the proposed device and those achieved with the digital refractometer. On the other hand, the ANN model aimed at estimating the grapes' TA displayed a similar performance, yielding an R^2 value of 0.67, and an RMSE of 0.83, which supposed the 16% of the mean value of the measurement (CVRMSE = 0.16). In this case, the CVRMSE value

indicated a lower predictive potential than what was obtained for the SSC. However, the results were also supported by the *p*-value obtained in the paired samples t-test ($p = 0.66$), which was also above than the significance limit. This indicated that there were no significant differences between the measures determined with the proposed device and those obtained through titration. The trends observed in the LOOCV were confirmed by the results obtained in the external validation of the random-sampling test for the SSC ($R^2 = 0.72$; RMSE = 1.10; CVRMSE = 0.07; $p = 0.20$) and TA estimation ($R^2 = 0.74$; RMSE = 0.84; CVRMSE = 0.17; $p = 0.53$). The few differences observed between the two validation methods are owed to the random division of the data set during the RS test.

In recent decades, there have been numerous studies concerning the characterization of horticultural products through machine-vision methods [3]. Concretely, the ripeness estimation in the viticulture sector has been widely studied, with works centred in different machine-vision techniques and ripening indicators [27,28]. In this sense, there have been numerous publications focused on the use of RGB images for estimating the ripening status of grapes, even under field conditions [29,30]. RGB colour imaging is a cost-effective way to determine colour channel values. In RGB colour imaging, however, only three visible bands are available, resulting in limited chemical composition identification capability. For this reason, most publications on the topic of RGB colour imaging for ripening-status assessment have been centred in classification models using subjective ripening indicators as reference, such as visual assessment [31,32]. Because these works used classification models with different performance criteria than were used in this research, it makes no sense to do an actual comparison. On the other hand, spectral sensors can record numerous bands across a wide spectral band. Further, spectroscopic features may better correlate with maturity since they are extracted from the absorption bands that are related to chemical attributes. Therefore, spectroscopy-based works rely on estimation models aimed at determining objective ripening indicators. In this sense, there are numerous works concerning the monitorization of grape-ripening using different spectroscopy-based techniques (VIS-NIR spectroscopy, hyperspectral imaging, multispectral imaging, etc.), and target parameters (SSC, TA, pH, flavonoids, anthocyanins, etc.). However, most of these works have been accomplished under laboratory conditions [24,33–37], where ambient light can be reasonably controlled by using a housing over the spectral system. This fact assumes an ease of use in contrast to spectrometers intended for in-vineyard use, such as the device proposed in this work. The shift of grape-composition measurements from the laboratory to the vineyard has become possible due to the advent of portable sensors and the rapid development of machine learning algorithms. An example of such an application is the work by Fernández-Novales et al. [38], who used a VIS–NIR hyperspectral camera (Resonon, Bozeman, MA, USA) (300 bans from 400 to 1000 nm) mounted on an all-terrain vehicle to acquire hyperspectral images from which to estimate the SSC and TA of grapes (along with other ripening parameters) using partial least squares regression (PLSR) models. They reported good correlations between the estimated and the measured values for the prediction of an external test set (SSC ($R^2 = 0.82$, RMSE = 1.21), TA ($R^2 = 0.81$, RMSE = 1.08)). Similarly, Guidetti et al. [39] used an experimental Vis/NIR spectrophotometer (AvaSpec-2048, Avantes, Eerbeek, The Netherlands) (450–980 nm) for estimating the SSC and TA of red grapes. They also used PLRS models for training and for external validation, obtaining an R^2 value of 0.67 and an RMSE of 1.48 for SSC, and an R^2 value of 0.66 and an RMSE of 1.48 for TA. On the other hand, Urraca et al. [40] used a portable NIR spectrophotometer (microPHAZIR™; Thermo Fisher Scientific, Waltham, MA, USA) (100 bands from 1595.7 to 2396.3 nm) for estimating the SSC of grapes under field conditions. They used a PLSR model as the retrieval method, which reported a 10-fold cross-validation R^2 up to 0.90 (with an RMSE of 1.47 Brix). The results obtained in the present work are comparable to those reported in the mentioned research. However, it is important to take into account that these works were performed using hyperspectral systems that offer a very high spectral resolution, which are capable of catching multiple narrow-spectral bands. This enables the acquisition of a more detailed spectral signature.

Therefore, the acquired spectral footprint of the target chemical parameter is more descriptive than what is obtained with multispectral devices using more expensive equipment. Furthermore, the NIR spectrophotometer used by Urraca et al. [40] covers the NIR domain with frequencies away from the red edge. In this region, several frequencies related to the SSC have been reported (1450, 1690, 1750, 1950, and 2260 nm (glucose)) [27]. However, the good correlation between the estimated and reference values of the SSC and TA founded in this work indicate that the spectral range considered is descriptive enough. This good performance may be due to the high flexibility of the ANN models, which adjust effectively in the feature space, as they enable the non-linearity of data to be modelled using local or specific equations. The aforementioned works used PLSR models to reduce the large amount of collinear spectral variables (offered by hyperspectral sensors) to non-correlated principal components by using data compression. On the other hand, it is important to take into account that the chemical analysis of grapes requires several berries per single sample (fifty berries per sample in this research). This implies that the sample unit must be comprised of the whole cluster. Thus, the variability concerning the ripening state in the berries of a cluster can constitute a source of error against studies focused on larger-size fruits. It is therefore possible to expect a better performance of the proposed device by evaluating such a type of fruit.

The results obtained in the present research take on a greater importance considering the price gap between the devices used in the previously mentioned research and the equipment proposed in this work. The performance showed by the proposed device, in addition to its price and the possibility to acquire measurement under field conditions, evince it as a promising and affordable solution to monitor grape-ripening status. The cost reduction achieved in the proposed design was possible due to the modernization of the electronics industry in recent decades. Improved hardware technology has provided sensors that deliver high performance at a reasonable price. Furthermore, innovative software designs offer algorithms that enhance the capacity to correlate the intricate relations that exist between spectral signatures and fruit biophysical parameters. This work, therefore, contributes to the trend toward the development of cheaper technologies with applications in precision agriculture [10,15,16].

5. Conclusions

This work presents the evaluation of a low-cost, multispectral sensor for grape-ripening-status assessment under field conditions. The performance achieved by the ANN models, fed with the spectral data acquired with the proposed device, shows a promising potential for the monitoring of grape ripening under field conditions. In-field monitoring, in addition to its price and ease of use, paves the way for the implementation of a fruit-ripening appraisal system that is affordable for all kinds of growers. The implementation of this technology in the vineyard would reduce laborious sampling and extensive chemical analysis for many workers. Furthermore, it would improve the spatiotemporal resolution in the monitorization, as it would increase both the number of sample points considered in each trial and the number of samples taken during the campaign. Moreover, the low cost of the sensor itself allows it to be integrated into wireless sensor networks or robotic devices. Regarding grapes, this device would enable the mapping of quality variability across the vineyard. It would therefore create opportunities to either exploit those variations to craft different wine styles or to apply precision viticultural techniques to optimize inputs and minimise variability. All of these factors would result in an increase in the expected market price of the wine produced. On the other hand, improving the accessibility of non-destructive and rapid technologies would improve the understanding of fruit maturation and how agronomic factors influence it.

The results obtained in the present work will encourage further work to expand this experimental setup to other grape varieties and other kinds of fruits.

Author Contributions: Conceptualization, M.N., B.M., and J.M.A.; data curation, M.N. and B.M.; formal analysis, M.N.; investigation, M.N.; methodology, M.N., B.M., and J.M.A.; project administration, B.M.; resources, B.M.; software, B.M.; supervision, B.M. and J.M.A.; validation, M.N.; visualization, B.M.; writing—original draft, M.N. and B.M.; writing—review & editing, J.M.A. All authors have read and agreed to the published version of the manuscript.

Funding: This work was supported by grant PID2020-119217RA-I00, funded by MCIN/AEI/ 10.13039/ 501100011033; grant IJC2019-040114-I, funded by MCIN/AEI/ 10.13039/501100011033; and grant 0766_OLIVAIS_5_E, funded by the Interreg Cooperation Program V-A SPAIN-PORTUGAL (POCTEP) 2014-2020, and co-financed with ERDF.

Institutional Review Board Statement: Not applicable.

Informed Consent Statement: Not applicable.

Data Availability Statement: The data presented in this study are available upon request from the corresponding author.

Acknowledgments: The authors acknowledge Bodegas Contreras Ruiz, S.L, for providing the experimental vineyard in which the study was conducted as well as the technical support. The authors also acknowledge Kimoto LDT for suppling the material used for making the light-diffuser film and the "Cátedra del Vino" from the University of Huelva for their support regarding chemical analysis.

Conflicts of Interest: The authors declare no conflict of interest. The funders had no role in the design of the study; in the collection, analyses, or interpretation of data; in the writing of the manuscript, or in the decision to publish the results.

References

1. López, M.I.; Sánchez, M.T.; Díaz, A.; Ramírez, P.; Morales, J. Influence of a deficit irrigation regime during ripening on berry composition in grapevines (*Vitis vinifera* L.) grown in semi-arid areas. *Int. J. Food Sci. Nutr.* **2007**, *58*, 491–507, https://doi.org/10.1080/09637480701311801.
2. Vanoli, M.; Buccheri, M. Overview of the methods for assessing harvest maturity. *Stewart Postharvest Rev.* **2012**, *8*, 1–11, https://doi.org/10.2212/spr.2012.1.4.
3. Cattaneo, T.M.P.; Stellari, A. Review: NIR Spectroscopy as a Suitable Tool for the Investigation of the Horticultural Field. *Agronomy* **2019**, *9*, 503, https://doi.org/10.3390/AGRONOMY9090503.
4. Lu, R.; Van Beers, R.; Saeys, W.; Li, C.; Cen, H. Measurement of optical properties of fruits and vegetables: A review. *Postharvest Biol. Technol.* **2020**, *159*, 111003, https://doi.org/10.1016/j.postharvbio.2019.111003.
5. Nicolaï, B.M.; Beullens, K.; Bobelyn, E.; Peirs, A.; Saeys, W.; Theron, K.I.; Lammertyn, J. Nondestructive measurement of fruit and vegetable quality by means of NIR spectroscopy: A review. *Postharvest Biol. Technol.* **2007**, *46*, 99–118, https://doi.org/10.1016/j.postharvbio.2007.06.024.
6. Comino, F.; Ayora-Cañada, M.J.; Aranda, V.; Díaz, A.; Domínguez-Vidal, A. Near-infrared spectroscopy and X-ray fluorescence data fusion for olive leaf analysis and crop nutritional status determination. *Talanta* **2018**, *188*, 676–684, https://doi.org/10.1016/j.talanta.2018.06.058.
7. Guzmán, E.; Baeten, V.; Pierna, J.A.F.; García-Mesa, J.A. A portable Raman sensor for the rapid discrimination of olives according to fruit quality. *Talanta* **2012**, *93*, 94–98, https://doi.org/10.1016/j.talanta.2012.01.053.
8. Noguera, M.; Aquino, A.; Ponce, J.M.; Cordeiro, A.; Silvestre, J.; Arias-Calderón, R.; da Marcelo, M.E.; Jordão, P.; Andújar, J.M. Nutritional status assessment of olive crops by means of the analysis and modelling of multispectral images taken with UAVs. *Biosyst. Eng.* **2021**, *211*, 1–18, https://doi.org/10.1016/j.biosystemseng.2021.08.035.
9. Wang, Y.J.; Jin, G.; Li, L.Q.; Liu, Y.; Kianpoor Kalkhajeh, Y.; Ning, J.M.; Zhang, Z.Z. NIR hyperspectral imaging coupled with chemometrics for nondestructive assessment of phosphorus and potassium contents in tea leaves. *Infrared Phys. Technol.* **2020**, *108*, 103365, https://doi.org/10.1016/j.infrared.2020.103365.
10. Walsh, K.B.; Blasco, J.; Zude-Sasse, M.; Sun, X. Visible-NIR 'point' spectroscopy in postharvest fruit and vegetable assessment: The science behind three decades of commercial use. *Postharvest Biol. Technol.* **2020**, *168*, 111246, https://doi.org/10.1016/J.POSTHARVBIO.2020.111246.
11. Li, B.; Lecourt, J.; Bishop, G. Advances in Non-Destructive Early Assessment of Fruit Ripeness towards Defining Optimal Time of Harvest and Yield Prediction—A Review. *Plants* **2018**, *7*, 3, https://doi.org/10.3390/PLANTS7010003.
12. Walsh, K.B.; McGlone, V.A.; Han, D.H. The uses of near infra-red spectroscopy in postharvest decision support: A review. *Postharvest Biol. Technol.* **2020**, *163*, 111139, https://doi.org/10.1016/J.POSTHARVBIO.2020.111139.
13. Millan, B.; Velasco-Forero, S.; Aquino, A.; Tardaguila, J. On-the-go grapevine yield estimation using image analysis and boolean model. *J. Sensors* **2018**, *2018*, 14, https://doi.org/10.1155/2018/9634752.
14. Diago, M.P.; Aquino, A.; Millan, B.; Palacios, F.; Tardaguila, J. On-the-go assessment of vineyard canopy porosity, bunch and leaf exposure by image analysis. *Aust. J. Grape Wine Res.* **2019**, *25*, 363–374, https://doi.org/10.1111/AJGW.12404.

15. Bec, K.B.; Grabska, J.; Huck, C.W. Miniaturized NIR Spectroscopy in Food Analysis and Quality Control: Promises, Challenges, and Perspectives. *Foods* **2022**, *11*, 1465, https://doi.org/10.3390/foods11101465.
16. Krause, J.; Grüger, H.; Gebauer, L.; Zheng, X.; Knobbe, J.; Pügner, T.; Kicherer, A.; Gruna, R.; Längle, T.; Beyerer, J. SmartSpectrometer—Embedded Optical Spectroscopy for Applications in Agriculture and Industry. *Sensors* **2021**, *21*, 4476, https://doi.org/10.3390/s21134476.
17. Noguera, M.; Millan, B.; Aquino, A.; Andujar, J.M. Methodology for Olive Fruit Quality Assessment by Means of a Low-Cost Multispectral Device. *Agronomy* **2022**, *12*, 979, https://doi.org/10.3390/agronomy12050979.
18. Moinard, S.; Brunel, G.; Ducanchez, A.; Crestey, T.; Rousseau, J.; Tisseyre, B. Testing the potential of a new low-cost multispectral sensor for decision support in agriculture. *Precis. Agric.* **2021**, *21*, 411–418, https://doi.org/10.3920/978-90-8686-916-9_49.
19. Zhang, M.; Shen, M.; Pu, Y.; Li, H.; Zhang, B.; Zhang, Z.; Ren, X.; Zhao, J. Rapid Identification of Apple Maturity Based on Multispectral Sensor Combined with Spectral Shape Features. *Horticulturae* **2022**, *8*, 361, https://doi.org/10.3390/horticulturae8050361.
20. Leon-salas, W.D.; Rajendran, J.; Vizcardo, M.A.; Postigo-malaga, M. Measuring Photosynthetically Active Radiation with a Multi-Channel Integrated Spectral Sensor. In Proceedings of the 2021 IEEE International Symposium on Circuits and Systems (ISCAS), Daegu, Republic of Korea, 23–26 May 2021; IEEE Xplore: Piscataway, NJ, USA, 2021; pp. 1–5.
21. Trang, N.M.; Duy, T.K.; Huyen, T.T.N.; Danh, L.V.Q.; Dinh, A. An investigation into the use of a low-Cost NIR integrated circuit spectrometer to measure chlorophyll content index. *Int. J. Innov. Technol. Explor. Eng.* **2019**, *8*, 35–38.
22. Li, M.; Qian, Z.; Shi, B.; Medlicott, J.; East, A. Evaluating the performance of a consumer scale SCiO™ molecular sensor to predict quality of horticultural products. *Postharvest Biol. Technol.* **2018**, *145*, 183–192, https://doi.org/10.1016/j.postharvbio.2018.07.009.
23. de Toda Fernández, M. *Claves de la Viticultura de Calidad: Nuevas Técnicas de Estimación y Control de la Calidad de la Uva en el Viñedo*, 2nd ed.; Ediciones Mundi-Prensa: Madrid, Spain, 2011; ISBN 9788484764229.
24. Gomes, V.M.; Fernandes, A.M.; Faia, A.; Melo-Pinto, P. Comparison of different approaches for the prediction of sugar content in new vintages of whole Port wine grape berries using hyperspectral imaging. *Comput. Electron. Agric.* **2017**, *140*, 244–254, https://doi.org/10.1016/J.COMPAG.2017.06.009.
25. International Organisation of Vine and Wine. *Compendium of International Methods of Wine and Must Analysis*, 2020th ed.; International Organisation of Vine and Wine: Paris, France, 2020; ISBN 9782850380167.
26. Demšar, J.; Erjavec, A.; Hočevar, T.; Milutinovič, M.; Možina, M.; Toplak, M.; Umek, L.; Zbontar, J.; Zupan, B. Orange: Data Mining Toolbox in Python. *J. Mach. Learn. Res.* **2013**, *14*, 2349–2353.
27. Vrochidou, E.; Bazinas, C.; Manios, M.; Papakostas, G.A.; Pachidis, T.P.; Kaburlasos, V.G. Machine Vision for Ripeness Estimation in Viticulture Automation. *Horticulturae* **2021**, *7*, 282, https://doi.org/10.3390/HORTICULTURAE7090282.
28. Dambergs, R.; Gishen, M.; Cozzolino, D. A Review of the State of the Art, Limitations, and Perspectives of Infrared Spectroscopy for the Analysis of Wine Grapes, Must, and Grapevine Tissue. *Appl. Spectrosc. Rev.* **2014**, *50*, 261–278, https://doi.org/10.1080/05704928.2014.966380.
29. Nuske, S.; Nuske, S. Automated Assessment and Mapping of Grape Quality through Image-cased Color Analysis. *IFAC-PapersOnLine* **2016**, *49*, 72–78, https://doi.org/10.1016/j.ifacol.2016.10.014.
30. Rahman, A.; Hellicar, A. Identification of Mature Grape Bunches using Image Processing and Computational Intelligence Methods. In Proceedings of the 2014 IEEE Symposium on Computational Intelligence for Multimedia, Signal and Vision Processing (CIMSIVP), Orlando, FL, USA, 9–12 December 2014; IEEE Xplore: Piscataway, NJ, USA, 2014; pp. 1–6.
31. Cavallo, D.P.; Cefola, M.; Pace, B.; Logrieco, A.F.; Attolico, G. Non-destructive and contactless quality evaluation of table grapes by a computer vision system. *Comput. Electron. Agric.* **2019**, *156*, 558–564, https://doi.org/10.1016/J.COMPAG.2018.12.019.
32. Kangune, K.; Kulkarni, V.; Kosamkar, P. Grapes Ripeness Estimation using Convolutional Neural network and Support Vector Machine. In Proceedings of the 2019 Global Conference for Advancement in Technology (GCAT), Bangalroe, India, 18–20 October 2019; IEEE Xplore: Piscataway, NJ, USA, 2019; pp. 1–5.
33. Baiano, A.; Terracone, C.; Peri, G.; Romaniello, R. Application of hyperspectral imaging for prediction of physico-chemical and sensory characteristics of table grapes. *Comput. Electron. Agric.* **2012**, *87*, 142–151, https://doi.org/10.1016/J.COMPAG.2012.06.002.
34. Fernandes, A.M.; Franco, C.; Mendes-Ferreira, A.; Mendes-Faia, A.; da Costa, P.L.; Melo-Pinto, P. Brix, pH and anthocyanin content determination in whole Port wine grape berries by hyperspectral imaging and neural networks. *Comput. Electron. Agric.* **2015**, *115*, 88–96, https://doi.org/10.1016/J.COMPAG.2015.05.013.
35. Gabrielli, M.; Lançon-Verdier, V.; Picouet, P.; Maury, C. Hyperspectral Imaging to Characterize Table Grapes. *Chemosensors* **2021**, *9*, 71, https://doi.org/10.3390/CHEMOSENSORS9040071.
36. Piazzolla, F.; Amodio, M.L.; Colelli, G. Spectra evolution over on-vine holding of Italia table grapes: Prediction of maturity and discrimination for harvest times using a Vis-NIR hyperspectral device. *J. Agric. Eng.* **2017**, *48*, 109–116, https://doi.org/10.4081/JAE.2017.639.
37. Fernández-Novales, J.; López, M.-I.; Sánchez, M.-T.; García-Mesa, J.-A.; González-Caballero, V. Assessment of quality parameters in grapes during ripening using a miniature fiber-optic near-infrared spectrometer. *Int. J. Food Sci. Nutr.* **2009**, *60*, 265–277, https://doi.org/10.1080/09637480903093116.
38. Fernández-Novales, J.; Barrio, I.; Diago, M.P. Non-invasive monitoring of berry ripening using on-the-go hyperspectral imaging in the vineyard. *Agronomy* **2021**, *11*, 2534, https://doi.org/10.3390/AGRONOMY11122534.

39. Guidetti, R.; Beghi, R.; Bodria, L. Evaluation of Grape Quality Parameters by a Simple Vis/NIR System. *Am. Soc. Agric. Biol. Eng.* **2010**, *53*, 477–484, https://doi.org/10.13031/2013.29556.
40. Urraca, R.; Sanz-Garcia, A.; Tardaguila, J.; Diago, M.P. Estimation of total soluble solids in grape berries using a hand-held NIR spectrometer under field conditions. *J. Sci. Food Agric.* **2016**, *96*, 3007–3016, https://doi.org/10.1002/jsfa.7470.